JCTC Journal of Chemical Theory and Computation

Mobile Block Hessian Approach with Adjoined Blocks: An Efficient Approach for the Calculation of Frequencies in Macromolecules

A. Ghysels,[†] V. Van Speybroeck,[†] E. Pauwels,[†] D. Van Neck,[†] B. R. Brooks,[‡] and M. Waroquier*,[†]

Center for Molecular Modeling, Ghent University, Proeftuinstraat 86, B-9000 Gent, Belgium, and Laboratory of Computational Biology, National Heart Lung and Blood Institute, National Institutes of Health, Bethesda, Maryland 20892

Received November 11, 2008

Abstract: In an earlier work, the authors developed a new method, the mobile block Hessian (MBH) approach, to accurately calculate vibrational modes for partially optimized molecular structures [*J. Chem. Phys.* 2007, *126* (22), 224102.]. It is based on the introduction of blocks, consisting of groups of atoms, that can move as rigid bodies. The internal geometry of the blocks need not correspond to an overall optimization state of the total molecular structure. The standard MBH approach considers free blocks with six degrees of freedom. In the extended MBH approach introduced herein, the blocks can be connected by one or two adjoining atoms, which further reduces the number of degrees of freedom. The new approach paves the way for the normal-mode analysis of biomolecules such as proteins. It rests on the hypothesis that low-frequency modes of proteins can be described as pure rigid-body motions of blocks of consecutive amino acid residues. The method is validated for a series of small molecules and further applied to alanine dipeptide as a prototype to describe vibrational interactions between two peptide units; to crambin, a small protein with 46 amino acid residues; and to ICE/caspase-1, which contains 518 amino acid residues.

I. Introduction

Conformational changes of macromolecules can be probed by a variety of experimental techniques such as X-ray crystallography, NMR spectroscopy, and so on.[1−4] The theoretical prediction of conformational flexibility is far from straightforward, especially for very large molecules such as proteins. In many cases, collective motions are present that occur on a time scale that is too long (on the order of milliseconds) to be accessible through molecular dynamics simulations.[5,6] Normal mode analysis (NMA) has proven successful in representing domain and hinge-bending motions in proteins, and it has been shown that, for several systems, the lowest-frequency modes contribute the most to conformational changes.

Until recently, theoretical studies of dynamical properties by NMA were restricted to rather small proteins.[7] This is partly due to the fact that a standard NMA needs to be preceded by an energy minimization. Because of the size of biological systems, this is already a computationally exhausting task. In addition, an NMA requires the diagonalization of a $3N_a \times 3N_a$ matrix (where N_a is the number of atoms). As the system becomes larger, this too becomes computationally very expensive.

A series of models has been proposed to simplify both the potential energy function[8] and the normal mode equations. For a detailed description, we refer to a recent review by Tama.[9] In particular, the method introduced by Durand et al.[10] and later extensively tested by Tama et al.[11] on relatively large biosystems (up to citrate synthase with 856 residues) deserves attention. It makes use of the concept that a protein chain can be seen as a sequence of rigid components, i.e., the peptide units. The combination of rotation

* Corresponding author e-mail: Michel.Waroquier@UGent.be.
[†] Ghent University.
[‡] National Institutes of Health.

10.1021/ct800489r CCC: $40.75
Published on Web 03/30/2009

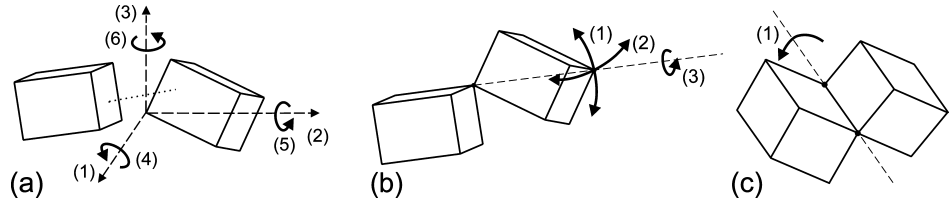

Figure 1. Degrees of freedom in the relative motion of (nonlinear) adjoined blocks. (a) Nonadjoined blocks have six degrees of freedom. The dotted line visualizes the bonding/nonbonding interaction between the blocks. (b) Blocks linked by one adjoining atom have three degrees of freedom. (c) Blocks linked by two adjoining atoms (hinge-type connection) have one degree of freedom.

and translation motions of these rigid blocks already gives a fair description of the lowest-frequency modes. For that reason, Tama et al. referred to this method as the RTB method, which stands for Rotations−Translations of Blocks.[11] In the approach developed by Durand et al.,[10] the possibility exists to obtain, in a second step, the exact normal modes by an iterative procedure, using effective Hamiltonians that couple the RTB modes with the higher-frequency internal modes of each block. This approach, however, might be problematic for larger systems, as one deals with a highly degenerate low-frequency spectrum in this case. Tama et al. showed that a good approximation of the lowest-frequency spectrum could already be obtained by performing only the first step.

Recently, we developed the mobile block Hessian (MBH) approach, which, in a sense, very much resembles the RTB method developed by Durand et al., as each block is allowed to move with six degrees of freedom attributed to translation and rotation.[12−14] The main difference between our original MBH method and the RTB method lies in the fact that the MBH method can also handle partially optimized systems. This kind of system also frequently occurs in other application fields, such as reactions taking place in porous materials or on surfaces. In that case, only part of the system is optimized, i.e., the chemically active part, whereas the rest is kept fixed to prevent unphysical deformations of the molecular environment. As a consequence of the partial optimization, the Hessian will have only three zero eigenvalues instead of six, implying that the rotational invariance of the potential surface is no longer manifest. Moreover, a set of spurious imaginary frequencies might appear.[12] In 2002, Li and Jensen introduced the partial Hessian vibrational analysis (PHVA) method, in which the fixed atoms are given an infinite mass during the frequency calculation and thus can no longer participate in the small-amplitude vibrations.[15] This method was successfully applied by Besley and Metcalf to calculate the amide I band of polypeptides and proteins.[16] More sophisticated schemes were introduced by Head and co-workers that allowed coupling between PHVA modes and modes in the fixed part.[17−20]

In this work, we introduce an extension of our original MBH method, in which the blocks can be linked to each other by one or two common atoms (adjoining atoms), as schematically shown in Figure 1. This is important, for instance, in very large (bio)systems, where one would like to have the possibility of calculating specific normal modes at decreased computational cost, as the number of degrees of freedom is further reduced by the introduction of adjoining atoms. If the blocks are linked by one atom, the block has three rotational degrees of freedom with respect to a previous block. If the blocks are linked by two atoms (creating a hinge-type connection), only one degree of freedom for the connected block remains. The linkage between blocks is a fundamental difference from the RTB method. Moreover, the MBH method is valid for partially optimized systems, even in the present adjoined version, extending the possible applications.

The newly introduced method is first tested on some basic test examples such as dimethylether and isobutane by assessing whether the system with reduced dimensionality can reproduce the original benchmark frequencies and associated normal modes. The hinge-type connection is tested for a series of *n*-alkanes and cyclohexane. Furthermore, the method is validated on a frequently investigated test example, alanine dipeptide, containing two peptide bonds. Finally, both connection schemes for the blocks are tested for crambin, a small protein with 46 amino acids. This system serves as a good test case because the MBH results can be compared to other methods that have also been tested on this polypeptide. To illustrate the ability of the MBH approach to treat quite large systems, the method is applied to ICE/caspase-1 with 518 amino acids.

II. Theoretical and Computational Approach

A. MBH Partitioning of the System. We distinguish among three different partitioning schemes, as illustrated in Figure 1. In the original implementation of the MBH method, atoms could only be part of one MBH block (a). In the current MBH approach, atoms can be part of two or more rigid blocks. Such a common atom, i.e., an adjoining atom, plays the role of a joint between the blocks. Two basic linkages can be realized with adjoining atoms: blocks connected by one adjoining atom (b) and blocks connected by two adjoining atoms (c). Unlinked blocks have six degrees of freedom in their relative motion, but blocks connected by an adjoining atom have only three (the three translational degrees of freedom are lost). The remaining three degrees of freedom correspond to rotations about an axis through the adjoining atom. If blocks are connected by two adjoining atoms to a previous block, the linkage is a hinge-type connection. Only one degree of freedom remains, corresponding to a rotation about the axis through the two adjoining atoms.

The hinge-type connection can correspond to some typical internal motions in molecules, as illustrated in Figure 2. The

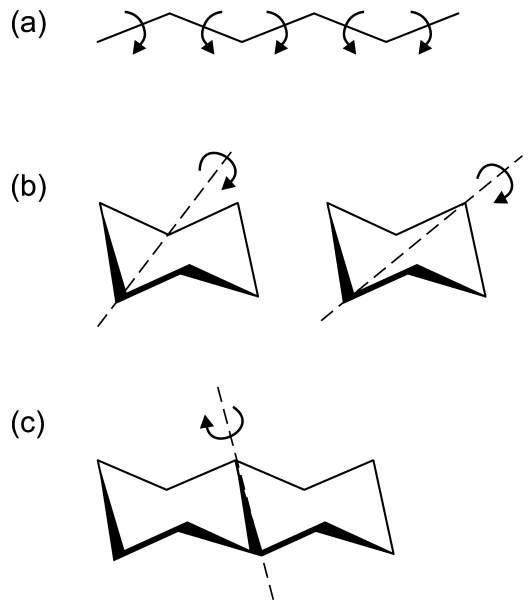

Figure 2. Three categories of motion characterized as involving hinge-type connections: (a) internal rotations, (b) ring inversion, (c) bending mode of two rings with respect to each other.

most important case (a) corresponds to internal rotations about a bond and occurs very frequently in chemistry. The hinge is determined by the atoms defining the rotational axis, i.e., by the chemical bond. Internal rotations in a molecule have frequently been studied in the literature, as they can show strong anharmonic motions.[21−27] The second case (b) can be found in ring compounds, in which ring inversions can take place. The hinge is defined in this case by two atoms that are not directly connected by a chemical bond. The third case (c) is found in fused ring systems where two rings can bend with respect to each other. Here, the hinge corresponds to the single bond that is common to the two rings.

B. Computational Details. Preference was given to the use of one single molecular mechanics program package, even for the small test molecules. The aim of the work was not the accurate reproduction of experimental frequencies for the relevant modes, but a validation of the MBH method with respect to full Hessian (benchmark) NMA. All calculations were performed with the PARAM22/27 (proteins) and PARAM34 (alkanes, ethers) force fields of the CHARMM package.[28] First, the geometry was fully optimized (root-mean square of the gradient lower than 10^{-6} kcal mol^{-1} Å^{-1}). For the dimethylether test case, two partially optimized geometries were generated as well using the SHAPE and restraints commands (RESD) from the CONS module. Next, the full Hessian was calculated in CHARMM and diagonalized with the VIBRAN module to obtain the benchmark (full Hessian) frequencies and modes.

C. Implementation. The extension of the MBH method to the case of adjoined blocks was implemented using a restraint technique and dummy atoms. This approach has the advantage that none of the MBH formulas in ref 13 need be changed. Only the Hessian must be complemented to impose the constraints. The procedure works for an arbitrary number of adjoining atoms connecting an arbitrary number of blocks,

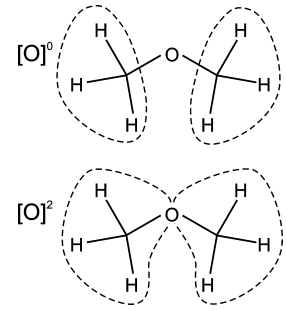

Figure 3. Dimethylether: Block choices.

so both linkages with one adjoining atom and linkages with two adjoining atoms can be treated.

Suppose an adjoining atom A belongs to s_A blocks. We can formally replace the adjoining atom by s_A dummy atom copies, A_1, ..., A_{s_A}, at the same reference position. The mass of the dummy atoms is the original mass m_A divided by s_A. Each of the dummy atoms is assigned to one of the blocks. In this way, a strict partition (no adjoining atoms anymore) of the atoms over the blocks is restored, and the former MBH computational routines can be used.

We must still impose the fact that the dummy copies, in reality, describe the same adjoining atom A, i.e., during the motion, the coordinates $\boldsymbol{r}_{A_1} = \cdots = \boldsymbol{r}_{A_{s_A}}$ should coincide. This can be done by adding to the potential energy harmonic terms of the form

$$V_A = \frac{1}{2}\kappa \sum_{i=2}^{s_A} |\boldsymbol{r}_{A_1} - \boldsymbol{r}_{A_i}|^2 \qquad (1)$$

for each adjoining atom. Choosing the spring constant κ sufficiently large will ensure that, during the motion, the positions of the dummy copies (nearly) coincide; otherwise, a large energy penalty is generated. At the level of the normal modes, the introduction of the dummy copies will lead to more vibrations than in the true system. However, the addition of the V_A terms to the potential energy will result in a clear energy separation between the physical modes where the dummy atoms coincide and the unphysical modes involving stretches between dummy copies of the same atom. These unphysical modes are all at much higher energies and can be easily deleted from the frequency list.

The value of κ to be used depends on the following considerations: On one hand, κ must be in the decoupling regime, so that the frequency spectrum of the physical modes does not depend on its value. On the other hand, an exageratedly large value for κ can lead to numerical instability as the condition number of the Hessian matrix deteriorates. In practice, a value of about 10^7 hartree/(Bohr length)^2 was found to provide excellent results.

In the following discussion, the share number s_A is used to label the different block choices. For instance, in Figure 3, $[O]^2$ specifies the block choice where the oxygen atom belongs to two blocks.

III. Results and Discussion

A. Small Test Molecules for Blocks Linked by One Adjoining Atom. *1. Dimethylether.* A first test case is

Table 1. Dimethylether: Frequency Calculations with the Fully Optimized Structure and Two Partially Optimized Structures[a,b]

fully optimized					partially optimized $[O]^0$		partially optimized $[O]^2$	
	blocks					blocks		blocks
full	$[O]^0$		$[O]^2$		full	$[O]^0$	full	$[O]^2$
0	0		0		−28	0	0	0
0	0		0		0	0	0	0
0	0		0		0	0	0	0
0	0		0		0	0	59	0
0	0		0		12	0	156	0
0	0		0		58	0	193	0
177	177	(100)	178	(100)	199	176	250	175
244	245	(100)	245	(100)	257	248	323	232
478	479	(100)	497	(98)	482	483	496	480
898	931	(97)			897	932	975	
1023	1061	(94)			1027	1061	1111	
1096	1135	(91)			1094	1136	1118	
1149	1201	(86)			1145	1203	1363	
1149	1209	(86)			1156	1212	1405	
1204	1244	(87)			1216	1247	1430	
1437					1443		1449	
1442					1445		1471	
1442					1450		1576	
1460					1463		2099	
1583					1571		2100	
1597					1585		2176	
2850					2848		2849	
2850					2849		2914	
2912					2912		2916	
2913					2913		5423	
2915					2915		5434	
2916					2919		5644	

[a] For each structure, the full Hessian (full) frequencies are compared with the MBH (blocks) frequencies, in cm^{-1}, including the frequencies due to global translation/rotation. [b] Maximum square overlap, $|\langle \nu^{MBH}|\nu^{bench}\rangle|^2$, given in parentheses (in %).

dimethylether. The full Hessian spectrum of the fully optimized structure has 21 normal modes in addition to the six global translational and rotational modes and serves as the benchmark (Table 1). The three lowest modes of dimethylether correspond to rotations of the methyl groups about an axis through the oxygen atom. Two block choices are considered as depicted in Figure 3. A natural choice is to put the methyl groups in two blocks, whereas the O atom in the center is a free atom not belonging to any block: $[O]^0$. This block choice corresponds to the original MBH approach. The number of degrees of freedom can be further reduced by omitting the stretch between the oxygen atom and the methyl groups. This is realized in block choice $[O]^2$, where the oxygen atom is taken up in both blocks. Table 1 lists the MBH frequencies, with the maximum square overlap with the benchmark, $|\langle \nu^{MBH}|\nu^{bench}\rangle|^2$, given in parentheses.

The results from the full optimization are discussed first. The MBH frequencies for block choice $[O]^0$ lie close to the benchmark, and the overlap values are larger than 86%. Only nine intrinsic normal modes remain, originating from the six degrees of freedom for each block, plus three translational degrees of freedom for the oxygen, minus the six global rotational and translational degrees of freedom. In the case of $[O]^2$, the oxygen atom acts as an adjoining atom between the two blocks. As a consequence, the C—O stretches no longer appear in the spectrum. Only three modes remain, which describe exactly the lowest normal modes with excellent overlaps of 98−100%. The value of the third lowest frequency has increased (497 cm^{-1}) because adjoining blocks increase the stiffness of the system, thereby giving rise to higher frequencies.

The last four columns of Table 1 show frequencies calculated for partially optimized structures. These were obtained in the following way: First, an initial nonequilibrium geometry was generated by disturbing the positions of some of the atoms by 0.1 Å from their global equilibrium positions. After the blocks had been defined (in this specific application, we considered $[O]^0$ and $[O]^2$), an energy minimization was performed with the internal coordinates within each block frozen. This led to a partially optimized structure. The individual atoms of the blocks might feel residual forces, but the positions and orientations of the blocks are optimized with respect to each other. For the thus-obtained partially optimized structure (which is different for each specific block choice), both a full Hessian calculation (column labeled "full") and an MBH calculation (column labeled "blocks") were carried out.

Partial optimization reduces the computation time for the geometry optimization; however, a standard full Hessian calculation on partially optimized structures might yield spurious low or even imaginary frequencies (indicated as negative values in Table 1). Also, unrealistically high frequencies can be detected in the vibrational spectrum (ca. 5000 cm^{-1}). Application of the MBH avoids such unphysical results. Moreover, the MBH frequencies from the partially optimized structures closely resemble those from the fully optimized structure, as can be seen in Table 1. The present MBH approach is therefore well-suited to treat partially

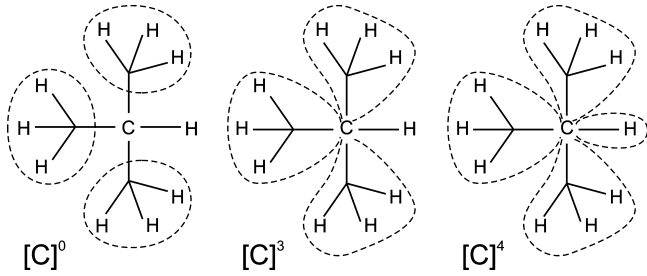

Figure 4. Isobutane: Block choices.

Table 2. Isobutane: Comparison of Benchmark (Full Hessian) and MBH Frequencies (cm^{-1}) for Different Block Choices[a]

	blocks					
full	[C]^0		[C]^3		[C]^4	
248	248	(100)	248	(100)	248	(100)
263×2	263	(100)	263	(100)	263	(100)
361×2	363	(100)	373	(99)	373	(99)
428	430	(100)	456	(97)	458	(97)
795	800	(99)				
917×2	928	(98)				
959×2	977	(97)				
961	978	(97)				
1117	1133	(96)				
1139×2	1149	(97)				
1356×2	1364	(89)	1258	(51)	1258	(51)
1399×2						
1400						
1426						
1429×2						
1435×2						
1436						
2901×3						
2944	2947	(79)	2916	(77)		
2957						
2958×2						
2960×2						
2963						

[a] Maximum (summed if degenerate modes) square overlap, $|\langle \nu^{MBH}|\nu^{bench}\rangle|^2$, given in parentheses (in %).

optimized structures. This simple test molecule illustrates that well-chosen adjoined blocks provide an economical way to reproduce interesting low-frequency normal modes.

2. Isobutane. As a second test case, we consider isobutane, where one can choose multiple adjoined blocks, all connected through the central carbon atom that serves as the adjoining atom. All investigated block choices are depicted in Figure 4. Case [C]^0 corresponds to nonadjoined blocks, whereas cases [C]^3 and [C]^4 include linkages. Table 2 compares the MBH results with the benchmark (full Hessian) spectrum. Isobutane has 12 degenerate benchmark frequencies because of the symmetry of the molecule. When calculating the maximum square overlap, we have taken into account this degeneracy by summing the square overlaps, $\sum_i |\langle \nu^{MBH}|\nu_i^{bench}\rangle|^2$, over the modes $|\nu_i^{bench}\rangle$ that belong to the same degenerate frequency ν^{bench} and picking the maximum summed square overlap.

Case [C]^0 with three methyl groups figuring as nonadjoined blocks yields good correspondence of the frequencies and also very good overlap of the modes (79% and higher). This is in full accordance with the previous MBH results reported in ref 12.

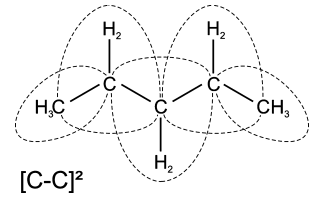

Figure 5. *n*-Alkanes: Block choice for pentane.

In the case of [C]^3, where the three methyl blocks are linked to each other by including the C atom in each of the three methyl blocks, the four lowest-frequency modes are very well reproduced by 97−100%. Some frequencies have increased with respect to the benchmark values because of the stiffening of the system. The remaining frequencies in the medium- and high-frequency spectrum, i.e., 1258 and 2916 cm^{-1}, correspond to motions of the free H atom (not belonging to any of the blocks): bending with respect to the three methyl groups and stretching of the C—H bond. Especially for the bending motion, the overlap is reduced, as this motion is expected to couple with the internal motions in the methyl block (steric hindrance hydrogens).

Case [C]^4 groups the H atom that was previously a free atom with the C atom into an additional linear adjoined block. Consequently, the C—H stretch is eliminated, whereas the rest of the frequencies and overlaps remain virtually unchanged. This illustrates the fact that the high-frequency stretch is not coupled to the lower-frequency spectrum. Such adiabatic behavior is the main justification for the use of constraints for the X—H bonds (N—H, O—H, etc.) in molecular dynamics simulations of extended (bio)systems (e.g., the SHAKE algorithm implemented in CHARMM[29]). The C—H stretches occur at a much shorter time scale and are not essential for configurational changes and other characteristics. Similarly, the C—H stretches are not relevant for the lower spectrum of the NMA, thereby justifying block choice [C]^4.

B. Small Test Molecules for Blocks Linked by Two Adjoining Atoms. *1. n-Alkanes.* Internal rotations belong to the category of hinge-type connections. We illustrate this by considering subsequent internal rotations in *n*-alkanes, going from propane to decane. Figure 5 shows how each C—CH_2—C unit forms a block, such that subsequent blocks always have the C—C bond in common. The blocks at the ends of the chain consist of a C—CH_3 unit. This block choice can be denoted by [C—C]^2, pointing out that each C—C bond belongs to two blocks. The only degrees of freedom that are not fixed by the partitioning are the dihedral angles of the internal rotations about the C—C bonds (see also Figure 2a).

Table 3 compares the MBH frequencies to the lowest full Hessian frequencies, which serve as the benchmark. The number of frequencies is reduced substantially from 9*n* (full) to only $n - 1$ frequencies, for a C_nH_{2n+2} alkane. Still, the MBH frequencies resemble the benchmark fairly well, and only a slight frequency enhancement is noticed, despite the rather drastic approximation. The overlap between MBH and full modes is 99% and higher, which means the lower spectrum of the *n*-alkanes is indeed built up of dihedral angle bending motions. Several gaps are noticed in the spectrum,

Table 3. Alkanes: Benchmark (Full Hessian) Frequencies[a] Compared to MBH Frequencies (cm^{-1})[b]

propane			butane			pentane			hexane		
full	[C—C]^2		full	[C—C]^2		full	[C—C]^2		full	[C—C]^2	
225	226	(100)	126	131	(100)	115	125	(100)	78	86	(99)
258	265	(99)	222	231	(99)	128	129	(100)	110	114	(99)
376			258	261	(100)	206			155		
⋯			293			244	249	(99)	161	167	(99)
			395			246	250	(100)	239	244	(99)
			⋯			356			249	254	(100)
						⋯			290		
									⋯		

heptane			octane			nonane			decane		
full	[C—C]^2		full	[C—C]^2		full	[C—C]^2		full	[C—C]^2	
61	69	(100)	46	52	(100)	38	43	(100)	30	35	(100)
89	91	(100)	79	81	(100)	68	70	(100)	62		
118			93			75			63	64	(100)
142	151	(99)	113	123	(99)	96	105	(99)	78	87	(100)
161	164	(100)	149	153	(99)	131	133	(100)	121	123	(100)
244	249	(99)	168	174	(100)	155	164	(99)	133	142	(99)
245	249	(100)	217			171	175	(100)	155		
265			243	248	(99)	187			165	169	(99)
277			246	250	(100)	210			171	177	(100)
⋯			246			244	244	(99)	193		
			363			245	250	(100)	244	244	(99)
			⋯			322			245	249	(100)
						⋯			272		
									⋯		

[a] Only lowest listed. [b] Maximum square overlap, $|\langle \nu^{MBH} | \nu^{bench} \rangle|^2$, given in parentheses (in %).

e.g., the third frequency of pentane (206 cm^{-1}) is missing, but visualization of this mode reveals that it mainly involves C—C—C angle bending, which is impossible to describe with the [C—C]^2 block choice. Summarizing, the study of *n*-alkanes demonstrates that the MBH approach with hinges captures the low-frequency modes associated with dihedral angle bending.

2. Cyclohexane. The hinge-type connection can also be used to select the rotation about an axis that does not coincide with a bond, as shown in Figure 2b, for instance, to describe puckering modes. This application is tested on the chair conformation of cyclohexane, which contains in the lower vibrational spectrum six ring bending modes at 232, 375, 439, and 547 cm^{-1}. The 232 and 438 cm^{-1} modes are doubly degenerate. These vibrational modes are schematically depicted in Figure 6a, for the hypothetical case that the molecule were planar. Modes 1−3 correspond to out-of-plane modes, whereas modes 4−6 correspond to (mainly) in-plane modes.[30] For the realistic nonplanar chair conformation of cyclohexane, the same terminology will be used but referring to the plane perpendicular to the 3-fold axis of the molecule. Various block choices were tested to investigate the extent to which the ring vibrations can be reproduced by the MBH approach (see Figure 6b). In the first case, [C1—C4]^2, the carbon ring is spit into two adjoined blocks using the hinge-type connection. The blocks can rotate with respect to each other about the common C1—C4 axis. The C—H stretches are eliminated by considering each C—H pair as a linear block connected to the ring. Equivalent splittings (because of the symmetry) have also been considered, i.e., [C2—C5]^2 and [C3—C6]^2. In the second case, [C1—C3]^2 + [C3—C5]^2 + [C5—C1]^2, the ring is split in three blocks, subsequently

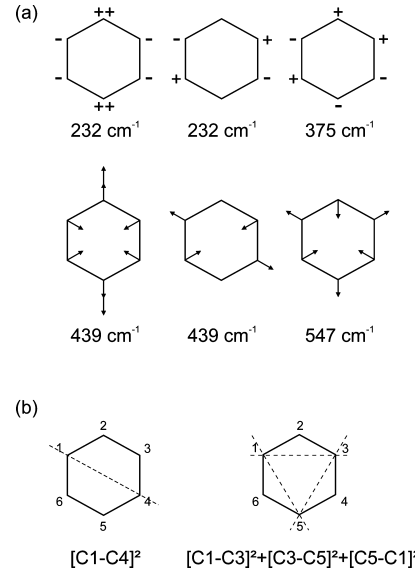

Figure 6. Planar representation of cyclohexane. (a) Six lowest-frequency bending modes. The first three are out-of-plane motions (±), and the next three are in-plane motions (arrows). (b) Block choices.

connected by one adjoining atom. This special case forms a ring structure of adjoined blocks.

The doubly degenerate mode at 439 cm^{-1} can never be reproduced accurately with our block choices (maximum square overlap of no more than 16%) because these correspond to C—C—C angle bendings. From the schematic representation of the modes in Figure 6, it can be anticipated that the last block choice is most suited to describe the 375 and 547 cm^{-1} modes. Both modes correspond to the flattening of the carbon ring. In the 375 cm^{-1} mode,

alternating CH_2 units rotate in opposite directions perpendicular to the plane. For the 547 cm^{-1} mode, the CH_2 units move in phase, and some C—C—C angle bending is involved. These modes can be best reproduced if the ring is split into three adjoined blocks (84% and 60%, respectively). One of the doubly degenerate 232 cm^{-1} modes coincides with the folding double motion and is indeed reproduced with the first block choice $[C1—C4]^2$ by 97%. The other 232 cm^{-1} mode represents a twist of the ring, which is a superposition of two folding double motions. Hence, the first block choice can only partially reproduce this mode (maximum square overlap of 74%). Splitting the ring into three blocks gives a better estimate of the mode, with a maximum square overlap of 84%.

This analysis illustrates how the nature of the complicated ring normal modes can be investigated with the MBH approach by examining the square overlaps. This is a useful feature, especially when the nature of the modes cannot be deduced uniquely by visualization. For the cyclohexane test case, it allowed us to confirm the nature of the six lowest bending modes.

C. Peptide Chains. *1. Block Choices.* The next step is to investigate whether the adjoined-blocks MBH model is appropriate for simulating the low-frequency modes of peptide chains. The peptide bond is known to be a stable planar unit, and it is straightforward to introduce blocks that include the entire peptide bond. Peptides have the ability to form different secondary structure elements as a result of the conformational flexibility of the backbone. There are essentially two backbone degrees of freedom for the amino acid residue: the dihedral angles ϕ (C—N—C_α—C) and ψ (N—C_α—C—N). The angles describe rotations about the N—C_α and C_α—C bonds, respectively.

Figure 7 provides an overview of the considered plausible partitioning schemes for peptide chains. The smallest block choice corresponds to considering consecutive peptide bonds (C═O—NH) as rigid blocks, labeled by $[C_\alpha]^0$. In case $[C_\alpha]^1$, a complete residue—peptide bond plus side chain—is considered as a block. This corresponds to the RTB approach introduced by Durand en al. and extensively tested by Tama et al. on a large variety of proteins.[10,11] From a methodological point of view, it corresponds to the MBH approach introduced in our earlier articles.[12−14] It is also possible to combine the adjoined blocks with atoms not included in any block. This is useful for the calculation of localized modes of interest, e.g., in the chemically active part. Such block choices have not been considered in this work.

The adjoined MBH approach allows the various blocks to be connected by one or more adjoining atoms. As a first approximation, the peptide units can be linked by the C_α atoms. This further reduces, by three, the total number of degrees of freedom for each considered block. Several options are possible for treating the side chain and the H atom connected to the C_α carbon, such as $[C_\alpha]^2$, $[C_\alpha]^{3a}$, $[C_\alpha]^4$, and $[C_\alpha]^{3b}$ in Figure 7, which will be discussed later with respect to the alanine dipeptide test case. Note that the actual block choice for the ends of the chain has little influence for long peptide chains.

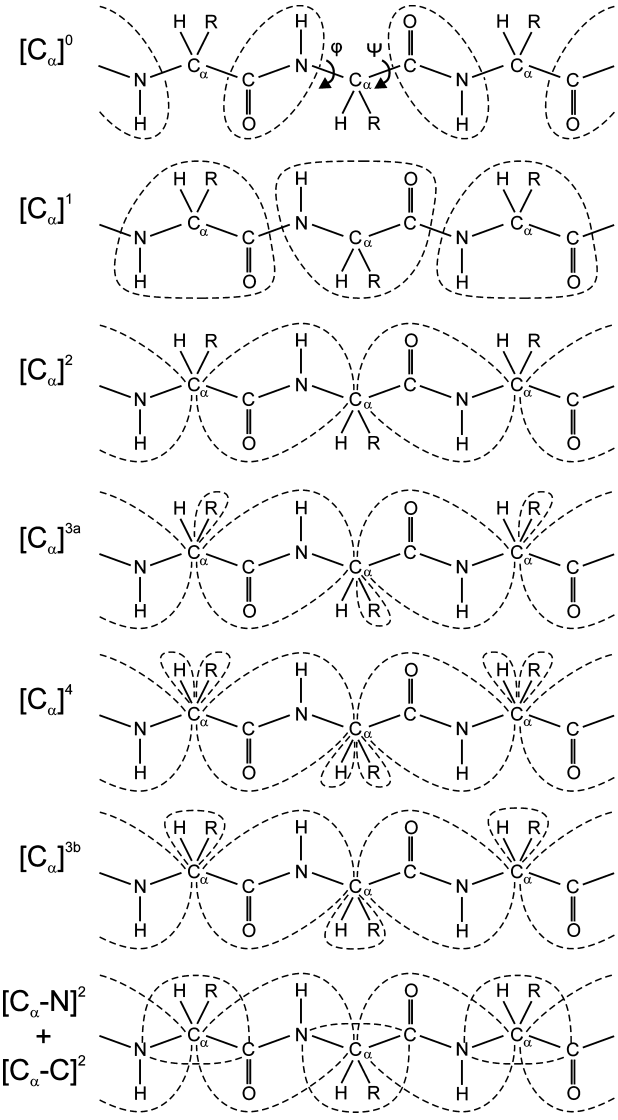

Figure 7. Partitioning schemes for peptide chains. Nonadjoined blocks: $[C_\alpha]^0$ and $[C_\alpha]^1$. Blocks linked by one adjoining atom: $[C_\alpha]^2$, $[C_\alpha]^{3a}$, $[C_\alpha]^4$, $[C_\alpha]^{3b}$. Blocks linked by two adjoining atoms: $[C_\alpha—N]^2 + [C_\alpha—C]^2$. Dihedral angles ϕ and ψ representing the two backbone degrees of freedom are also shown for the top chain.

Finally, the subsequent blocks can share two adjoining atoms as shown at the bottom of Figure 7. Each introduced block shares the C_α—N bond or the C_α—C with the block connecting the subsequent peptide units. As a result, the only degrees of freedom that are left over are the internal rotations about the common C_α—N and C_α—C bonds, which are exactly the ϕ and ψ dihedral angles. This block choice is labeled by $[C_\alpha—N]^2 + [C_\alpha—C]^2$, referring to the common C_α—N and C_α—C bonds.

By simply choosing adjoined blocks, as in $[C_\alpha—N]^2 + [C_\alpha—C]^2$, one is able to select the dihedral angles as variables. The MBH model is thus useful for NMA with variables of interest, without the need for extra computational implementations for the construction of the variables (i.e., no complicated transformation to internal coordinates is required). As for the geometry optimization, only the ϕ and ψ dihedral angles have to be force-free; other internal coordinates do not necessarily have to be optimized in the MBH

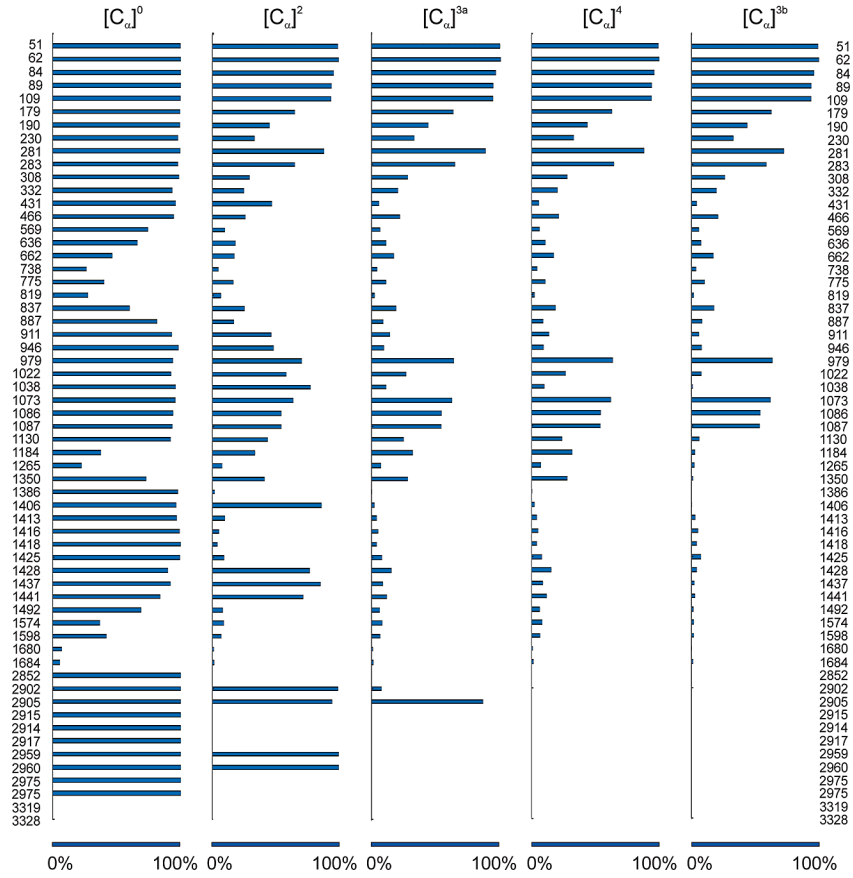

Figure 8. Alanine dipeptide: Cumulative square overlap P_j (%) for each non-zero-frequency benchmark mode.

framework. From a computational point of view, the reduction of the Hessian size is impressive. Only two degrees of freedom (ϕ, ψ) are considered per residue. A protein with N_R residues easily has over $30N_R$ degrees of freedom, but the adjoined blocks with hinges reduces this number to $2N_R$.

2. Alanine Dipeptide. Blocked (or capped) alanine dipeptide (N-acetyl-L-alanine-N′-methylamide) is commonly studied as a prototype of nonglycine/nonproline protein backbones, since it allows full sampling of the ϕ/ψ conformational space without the additonal complexity of side-chain degrees of freedom.[31] Numerous computational and experimental studies of alanine dipeptide have explored the thermodynamic,[32,33] kinetic[34−36] and spectroscopic properties.[37,38] Alanine dipeptide takes several conformations in gas phase.[39,40] In this study, the stable conformer with $\phi = -81°$ and $\psi = 70°$, usually referred to as $C7_{eq}$, was used.

To quantify how a benchmark normal mode, resulting from a full NMA analysis, corresponds to an MBH normal mode, the square overlap between the corresponding eigenvectors is again used. However, as the system size increases, many modes become degenerate or nearly degenerate. It is then more appropriate to use a cumulative square overlap P_j, defined as

$$P_j = \sum_i |\langle \nu_i^{\mathrm{MBH}} | \nu_j^{\mathrm{bench}} \rangle|^2 \qquad (2)$$

which quantifies how well the benchmark mode $|\nu_j^{\mathrm{bench}}\rangle$ can be reproduced by all MBH modes $\{|\nu_i^{\mathrm{MBH}}\rangle\}$. The overlap does not necessarily become 100% because the MBH modes do not form a complete basis.

The efficiency and adequacy of the adjoined MBH method are best illustrated by examining the cumulative square overlap P_j for each non-zero-frequency benchmark mode, as can be seen in Figure 8. The block choices $[C_\alpha]^2$, $[C_\alpha]^{3a}$, $[C_\alpha]^4$, and $[C_\alpha]^{3b}$ from Figure 7 are considered to investigate how the side chain should be treated. To allow a full comparative study the results of block choice $[C_\alpha]^0$, where the peptide units are considered as nonadjoined blocks, are also shown in the first column of Figure 8. The 14 lowest-frequency modes and the high-frequency C—H stretches are reproduced by the MBH modes for at least 97%. Only some of the modes in the medium-frequency range are less well reproduced.

In the next four cases, blocks are linked to each other with the C_α atom as the adjoining atom. The ending methyl groups are also considered as blocks adjoined to the peptide unit blocks. In the case of $[C_\alpha]^2$, the side-chain atoms and the hydrogen atom are still free atoms. The frequencies are overestimated as a result of the stiffening of the system, but the cumulative square overlap indicates that the five lowest benchmark modes are still more than 90% reproduced. Case $[C_\alpha]^{3a}$ further reduces the number of frequencies by considering the side chain as an adjoined block as well (only the hydrogen atom is a free atom). The overlap in the lower spectrum is almost not influenced.

In case $[C_\alpha]^4$, the C_α—H stretch is eliminated by grouping the C_α and hydrogen atom in yet another adjoined block, such that the C_α atom links four blocks. As expected from the isobutane discussion, this C_α—H stretch is not coupled to the rest of the spectrum, which remains unchanged. Fixing

the angle between the C_α—H block and the side-chain block leads to case $[C_\alpha]^{3b}$ where the H atom is added to the side-chain block. Results largely resemble the previous $[C_\alpha]^4$ case, except for some medium frequencies around ± 1100 cm^{-1} associated with the side chain-C_α—H bending.

This example shows that grouping the atoms of the side chain into an adjoined block is a suitable choice to reproduce the lowest-frequency modes. Moreover the side-chain C_α—H bending and the C_α—H stretch are irrelevant for the lower spectrum, and the hydrogen atom can be included in the side-chain block (block choice $[C_\alpha]^{3b}$). The MBH method with linked blocks therefore appears to be an appropriate analysis tool for the lower spectrum of peptide chains.

3. Crambin. The MBH method with adjoined blocks is next applied to a longer, more representative peptide chain with a variety of amino acids. As an example, the well-known protein crambin (Protein Data Bank 1CCN) is chosen. The crambin molecule contains three disulfide bonds and displays β-strand, β-turn, and helical elements of protein secondary structure. The structure of crambin in water as determined by 2D NMR spectroscopy[41] was taken as a starting point for the geometry optimization (in the absence of the solvent). Crambin has 46 residues, including 648 atoms, and hence, the full NMA would result in 1944 frequencies. It is our aim to reduce the number of frequencies drastically by performing an MBH analysis on the system, but still to preserve the essential lowest-frequency normal modes.

The first block choice $[C_\alpha]^0$ considers the peptide groups (C═O—NH) as nonadjoined blocks, which is realizable with the previous MBH implementation. The square overlaps (not shown) revealed that the peptide units indeed move as nearly rigid groups, even when some of the residues are heavier and the peptide chain is longer.

Subsequently, it is investigated whether blocks can be adjoined. Three block choices from the list in Figure 7 are proposed, of which the first already gave promising results in the previous section: (1) case $[C_\alpha]^{3b}$ groups the side chain and the H atom in an adjoined block, (2) case $[C_\alpha]^1$ is the scheme introduced by Tama et al., and (3) case $[C_\alpha—N]^2 + [C_\alpha—C]^2$ uses the hinge-type connection.

Figure 9 compares the low-frequency part of the benchmark (full Hessian) spectrum with the MBH results. A grayscale indicates the square overlap between the modes. A dot on the diagonal indicates an exact frequency estimation, and the darker the dot, the better the overlap. A huge number of frequencies (1944) lies in a limited frequency interval—between 0 and 4000 cm^{-1}—and therefore, the square overlaps seldomly reach high values because of degeneracy. The cumulative square overlap P_j does not depend on the degeneracy as it sums over all MBH frequencies. Figure 10 shows a plot of the values of P_j for the benchmark modes below 50 cm^{-1}. It indicates how well a benchmark mode is still represented by all MBH modes.

Block choice $[C_\alpha]^{3b}$ overestimates the frequencies because of the stiffening of the system, but the cumulative overlap shows that reproduction of the benchmark modes is very good in the low-frequency range: all but one of the benchmark modes below 50 cm^{-1} are reproduced for at least 90% by the MBH modes, which is largely sufficient. Block

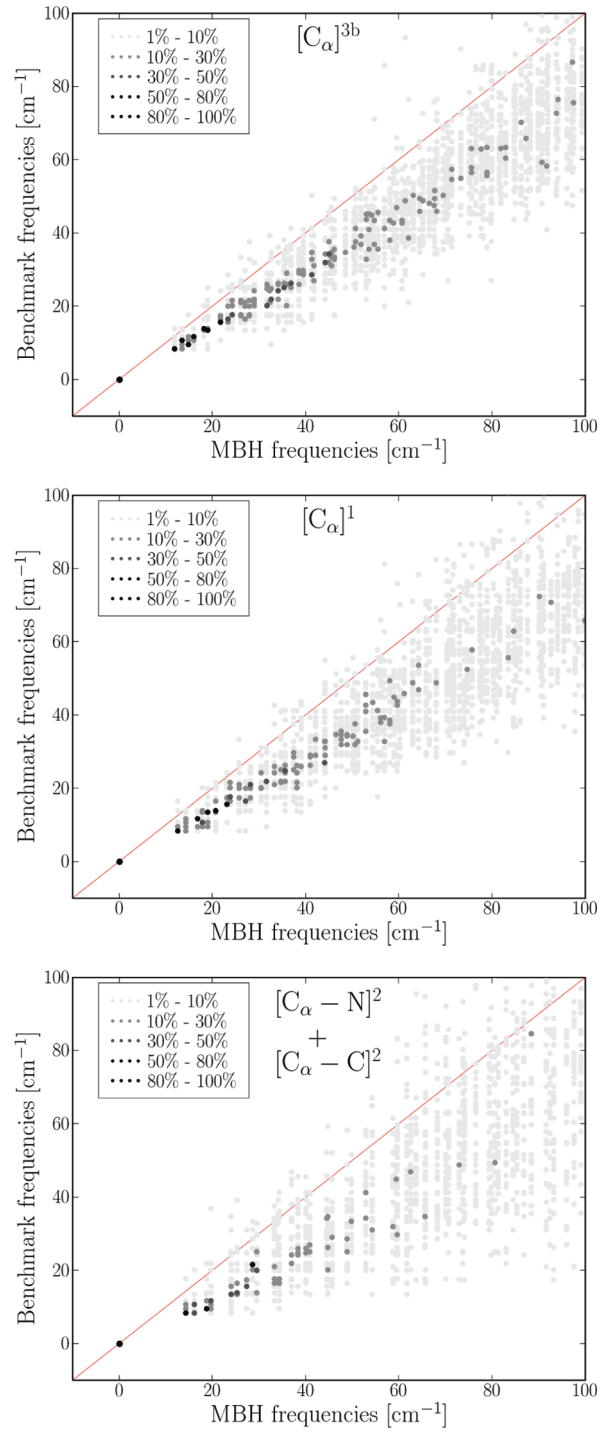

Figure 9. Crambin: Square overlap (%) between MBH modes and benchmark (full Hessian) modes in the 0−100 cm^{-1} frequency range for block choices $[C_\alpha]^{3b}$, $[C_\alpha]^1$, and $[C_\alpha—N]^2 + [C_\alpha—C]^2$.

choice $[C_\alpha]^{3b}$ differs from block choice $[C_\alpha]^4$ in the treatment of the H atom connected to the C_α carbon. Eliminating the C_α—H stretch without constraining the side chain C_α—H angle gives a somewhat more flexible model of the backbone, and case $[C_\alpha]^4$ is expected to be a more accurate approximation. However, the effect is minimal in the lower spectrum and becomes manifest only in the range above 250 cm^{-1} (not shown), because the H-atom motions interact very little with the backbone modes. Hence, when one is interested in the lowest frequencies, the side chain C_α—H angle bending

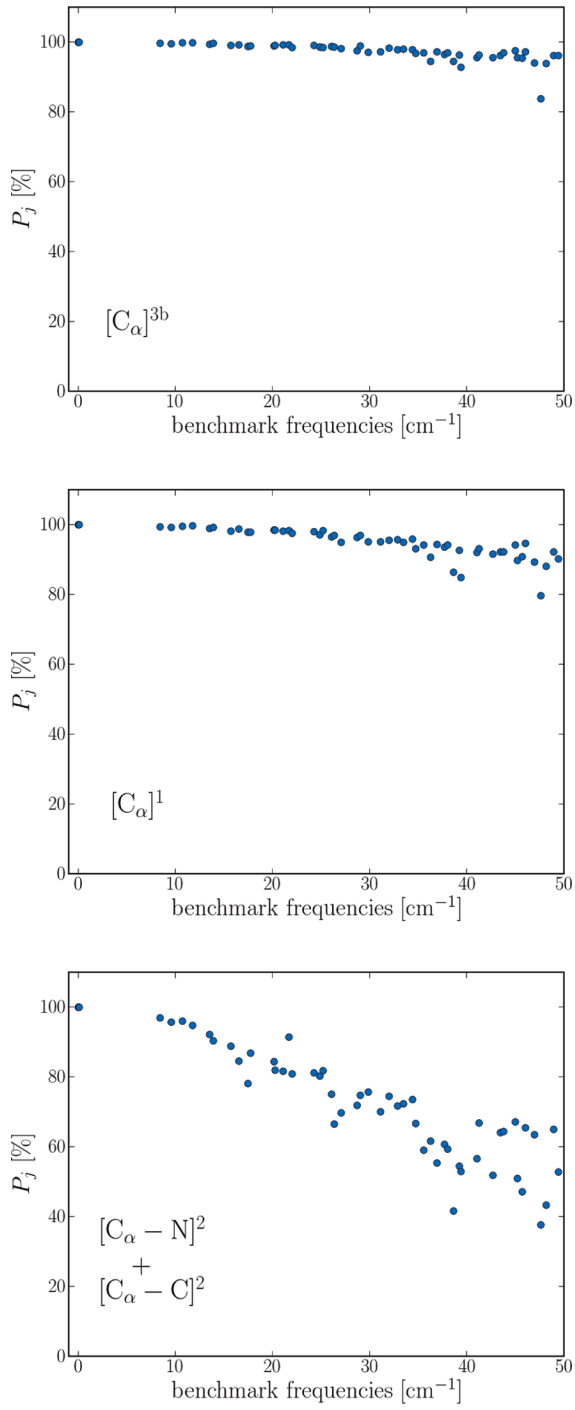

Figure 10. Crambin: Cumulative square overlap P_j (%) for benchmark modes in the 0−50 cm^{-1} range for block choices $[C_\alpha]^{3b}$, $[C_\alpha]^1$, and $[C_\alpha{-}N]^2 + [C_\alpha{-}C]^2$.

motion is not essential, and a partitioning as in case $[C_\alpha]^{3b}$, where all motions of the hydrogen atom are omitted, is sufficient.

The introduction of rigid blocks for the peptide chain implies a serious reduction of the number of degrees of freedom. In general, a peptide chain with N_{res} residues can be partitioned according to the $[C_\alpha]^{3b}$ block choice in a chain of N_{res} peptide blocks connected by the C_α atoms and N_{res} side-chain blocks linked to the chain by the C_α atoms as well. With three degrees of freedom per block, the total number becomes $6N_{res}$. For example, for crambin, the MBH method results in 276 modes, which is 14% of the initial 1944 variables.

A similar reduction was obtained by Tama et al.[11] with blocks consisting of several (n) peptide-plus-side-chain units. The blocks are not linked to each other, leading to a total number of $6N_{res}/n$ degrees of freedom. For comparison, we reproduced the overlap results in the case of one single peptide-plus-side-chain unit per block ($n = 1$). This partitioning, block choice $[C_\alpha]^1$ in Figure 7, gives the same reduction of modes as the $[C_\alpha]^{3b}$ partitioning with adjoined blocks. The overlap and cumulative overlap of $[C_\alpha]^1$ also perform well, although somewhat worse than the MBH approach with adjoined blocks. Thus, for the same degree of simplification, the introduction of adjoined blocks leads to a slight improvement of the partitioning proposed by Tama et al.

Tama et al. observed a linear relationship between the benchmark and the MBH frequencies

$$\nu_{MBH} = d\nu_{bench} \tag{3}$$

The factor d was obtained by a linear least-squares fit when comparing the lowest, say, n_{low}, benchmark modes with the n_{low} lowest MBH modes. For cases $[C_\alpha]^{3b}$ and $[C_\alpha]^1$, we find $d = 1.41$ and 1.49, respectively, when the lowest modes (below 40 cm^{-1}) are taken into account. The overestimation of the frequencies, i.e., $d > 1$, is due to the stiffening of the system. Applying the block constraints limits the motions to a hypersurface on the potential energy surface, which has higher curvatures than the total potential energy surface. In other words, the constraints make the system stiffer because the motion of blocks as a whole is more hindered than it would be if the atoms in the block were allowed to relax. On the other hand, the inertia of the blocks can lower the frequencies, because a block moving as a whole has more inertia than the atoms moving individually. The frequency change is thus governed by the balance between stiffening and inertia effects. The systematic frequency overestimation indicates that, in the lower spectrum of peptide chains, the stiffening is the dominating effect for the considered block choices.

The number of modes can be further reduced by using the partitioning scheme with hinges. The dihedral basis $[C_\alpha{-}N]^2 + [C_\alpha{-}C]^2$ as illustrated in Figure 7 was applied to crambin and reduced the number of modes to 96, which is as low as 4.9% of the initial number of variables. The results are again compared with the benchmark (full Hessian) frequencies in Figures 9 and 10.

The overlap plot indicates that fewer modes are reproduced and the frequency overestimation increases: $d = 1.85$. Still, the cumulative overlap P_j shows that 8 modes are reproduced by over 90%, whereas 20 modes are reproduced by over 80%. Visualization of the modes shows that the lowest MBH modes indeed represent large-amplitude motions where large parts of the chain move as a whole. The cumulative overlap decays rapidly when the frequency increases. In practice, of course, one usually investigates only the motions in the lowest five frequency modes for the purpose of analyzing conformational changes. Hence, it is clear that the simplification of block choice $[C_\alpha{-}N]^2 + [C_\alpha{-}C]^2$ still captures the

Table 4. Caspase-1: Lowest 14 Nonzero Benchmark (Full Hessian) Frequencies Compared to the Lowest MBH Frequencies (cm^{-1}), by Means of the Square Overlap $|\langle \nu^{MBH}|\nu^{bench}\rangle|^2$ (%)[a,b]

	benchmark													
MBH	3.4	3.6	3.9	4.8	5.4	5.4	5.7	5.7	5.8	5.8	6.0	6.5	6.6	7.3
6.5	11		**62**	21										
7.3	**25**			**61**										
7.6		**84**												
8.8					**33**	**46**								
9.2							**38**				**30**	18		
9.4					12	11		**42**		11				
9.6									**63**					
10.2							**38**				**34**			
10.6													**42**	
11.0					24			13					11	
11.9									11			**36**		
12.1														**63**
12.4										**46**				
12.6								13					11	
cum. sq. overlap	93	100	97	98	99	100	99	99	99	99	100	99	99	99

[a] Square overlaps below 10% are not shown; square overlaps above 25% are highlighted to emphasize the diagonal. [b] Cumulative square overlap P_j (%) given for each benchmark frequency at the bottom of the table.

essentials of the lowest modes and can be used as an analysis tool that focuses on the lower spectrum.

4. Caspase-1. To demonstrate the ability to treat quite large systems, we will briefly discuss the case of the interleukin-1 β converting enzyme (ICE or caspase-1, Protein Data Bank 1ICE).[42] This protein is a member of the caspase family of enzymes, which play a crucial role in apoptosis or programmed cell death. More specifically, caspase-1 proteolytically processes the interleukin-1β precursor to its active state and, hence, contributes essentially to the immune response.[43]

Caspase-1 is a tetramer, consisting of 518 residues and totaling 8252 atoms. A full Hessian diagonalization for the optimized structure would yield 24756 frequencies at a prohibitive expense. MBH with adjoined blocks considerably reduces the complexity to a fraction of the computational cost (less than 15%). For the calculation of the MBH frequencies, we made use of a recently developed method based on analytical constraints.[44] This method leads to the same numerical results as the dummy atom method described in section II but is much more efficient for extended molecular systems. The adjoined block choice $[C_\alpha]^{3b}$ was selected in view of its good performance in the crambin case. To show the potential of our MBH method, comparison was made with the 20 lowest exact full Hessian frequencies and modes, calculated with the DIAG option of CHARMM.

The six lowest frequencies correspond to the global translational and rotational modes. The next 14 nonzero modes lie in a narrow frequency range of 3.4−7.3 cm^{-1}, and their square overlaps with the lowest MBH frequencies, $|\langle \nu^{MBH}|\nu^{bench}\rangle|^2$, are given in Table 4. Square overlaps below 10% are not shown; square overlaps above 25% are highlighted. Because of the high degeneracy of the modes, the modes seem to be mixed up or to have changed order, but the highest square overlaps nevertheless lie close to the diagonal of the table. The cumulative square overlap P_j is given at the bottom of Table 4. Because P_j is consistently high with values of >93%, the MBH normal modes indeed represent adequate coordinates for the motions of the lower-frequency spectrum.

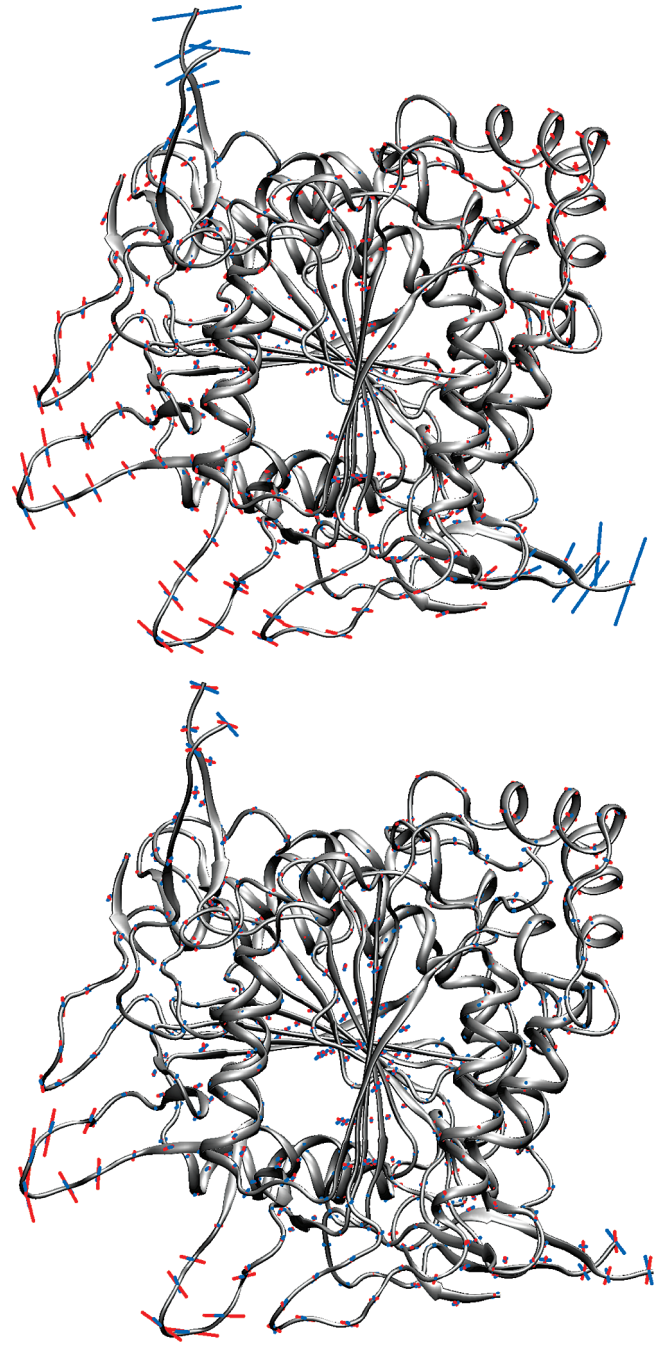

Figure 11. Caspase-1: Visualization of C_α movement in the MBH (red) and full (blue) normal modes. (top) First nonzero mode. (bottom) The fourth nonzero mode clearly shows movement of the caspase-1 subdomains with respect to each other.

The first nonzero full Hessian mode is not so well described by the lowest MBH modes. As illustrated in Figure 11, this mode is mainly active in sections where the C-terminal and N-terminal regions of two polypeptide chains meet. Other modes, on the other hand, are much better reproduced and describe more coherent, global motions of the subdomains with respect to each other.

IV. Conclusions

The extension of the MBH method to the case of adjoined blocks is a computationally attractive method for analyzing modes from the lower-frequency spectrum. The computational profit offered by the MBH with adjoined blocks can be exploited at two levels. First, during the energy minimization, fewer coordinates need to be optimized. Second, during the vibrational analysis, one needs to calculate fewer second derivatives, and the much smaller size of the adapted Hessian speeds up the diagonalization.

Testing the adjoined MBH model on several small test systems revealed that frequencies can be somewhat overestimated because of the stiffening of the system, but in general, the low-frequency normal modes are very well reproduced. The block choice is obviously crucial for the quality of the MBH frequencies and modes. By varying the block sizes, the MBH can therefore be used as an analysis tool for characterizing modes. By excluding several atoms from the blocks, MBH can also analyze the coupling between those atoms (e.g., the reactive site) and the surrounding blocks (the environment). The main application of the MBH model with adjoined blocks, however, is in the calculation of the lower spectrum of macromolecules. Especially for proteins, the MBH approach provides an efficient method to focus on the modes involved in conformational changes. Several block choices were examined for their ability to reproduce the low frequencies and modes. Among the adjoined block schemes, the $[C_\alpha]^{3b}$ block choice, where peptide units and side chains are grouped into blocks with C_α as the adjoining atom, performs well in reproducing the modes of relevance while reducing the number of modes considerably. In the $[C_\alpha{-}N]^2 + [C_\alpha{-}C]^2$ block choice, where only dihedral angles are retained as degrees of freedom, the reduction of the dimensionality is very large. The resulting modes are less accurate, but still reasonable. The MBH method with adjoined blocks therefore appears to be an appropriate analysis tool for the lower spectrum of peptide chains.

Acknowledgment. A.G. is Aspirant of the Fund for Scientific Research - Flanders (FWO). This work was supported by the Fund for Scientific Research - Flanders (FWO), the Research Board of Ghent University (BOF), and the Belgian Program on Interuniversity Attraction Poles (IAP).

References

(1) Xiao, M.; Reifenberger, J. G.; Wells, A. L.; Baldacchino, C.; Chen, L. Q.; Ge, P. H.; Sweeney, H. L.; Selvin, P. R. *Nat. Struct. Biol.* **2003**, *10* (5), 402–408.

(2) Ishima, R.; Torchia, D. A. *Nat. Struct. Biol.* **2000**, *7* (9), 740–743.

(3) Saibil, H. R. *Nat. Struct. Biol.* **2000**, *7* (9), 711–714.

(4) Rossmann, M. G.; Morais, M. C.; Leiman, P. G.; Zhang, W. *Structure* **2005**, *13* (3), 355–362.

(5) Elber, R. *Curr. Opin. Struct. Biol.* **2005**, *15* (2), 151–156.

(6) Schlick, T.; Barth, E.; Mandziuk, M. *Annu. Rev. Biophys. Biomol. Struct.* **1997**, *26*, 181–222.

(7) Case, D. A. *Curr. Opin. Struct. Biol.* **1994**, *4* (2), 285–290.

(8) Tirion, M. M. *Phys. Rev. Lett.* **1996**, *77* (9), 1905–1908.

(9) Tama, F. *Protein Pept. Lett.* **2003**, *10* (2), 119–132.

(10) Durand, P.; Trinquier, G.; Sanejouand, Y. H. *Biopolymers* **1994**, *34* (6), 759–771.

(11) Tama, F.; Gadea, F. X.; Marques, O.; Sanejouand, Y. H. *Proteins: Struct. Funct. Genet.* **2000**, *41* (1), 1–7.

(12) Ghysels, A.; Van Neck, D.; Van Speybroeck, V.; Verstraelen, T.; Waroquier, M. *J. Chem. Phys.* **2007**, *126* (22), 224102.

(13) Ghysels, A.; Van Neck, D.; Waroquier, M. *J. Chem. Phys.* **2007**, *127* (16), 164108.

(14) Ghysels, A.; Van Speybroeck, V.; Verstraelen, T.; Van Neck, D.; Waroquier, M. *J. Chem. Theory Comput.* **2008**, *4* (4), 614–625.

(15) Li, H.; Jensen, J. H. *Theor. Chem. Acc.* **2002**, *107*, 211–219.

(16) Besley, N. A.; Metcalf, K. A. *J. Chem. Phys.* **2007**, *126* (3), 035101.

(17) Calvin, M. D.; Head, J. D.; Jin, S. Q. *Surf. Sci.* **1996**, *345* (1−2), 161–172.

(18) Head, J. D. *Int. J. Quantum Chem.* **1997**, *65* (5), 827–838.

(19) Head, J. D.; Shi, Y. *Int. J. Quantum Chem.* **1999**, *75* (4−5), 815–820.

(20) Head, J. D. *Int. J. Quantum Chem.* **2000**, *77* (1), 350–357.

(21) Heuts, J. P. A.; Gilbert, R. G.; Radom, L. *J. Phys. Chem.* **1996**, *100* (49), 18997–19006.

(22) Van Speybroeck, V.; Van Neck, D.; Waroquier, M. *J. Phys. Chem. A* **2000**, *104* (46), 10939–10950.

(23) Van Speybroeck, V.; Van Neck, D.; Waroquier, M. *J. Phys. Chem. A* **2002**, *106* (38), 8945–8950.

(24) Van Speybroeck, V.; Vansteenkiste, P.; Van Neck, D.; Waroquier, M. *Chem. Phys. Lett.* **2005**, *402* (4−6), 479–484.

(25) Lynch, V. A.; Mielke, S. L.; Truhlar, D. G. *J. Phys. Chem. A* **2005**, *109* (44), 10092–10099.

(26) Vansteenkiste, P.; Van Neck, D.; Van Speybroeck, V.; Waroquier, M. *J. Chem. Phys.* **2006**, *124* (4), 044314.

(27) Pfaendtner, J.; Yu, X.; Broadbelt, L. J. *Theor. Chem. Acc.* **2007**, *118*, 881–898.

(28) Brooks, B. R.; Bruccoleri, R. E.; Olafson, B. D.; States, D. J.; Swaminathan, S.; Karplus, M. *J. Comput. Chem.* **1983**, *4* (2), 187–217.

(29) Vangunsteren, W. F.; Berendsen, H. J. C. *Mol. Phys.* **1977**, *34* (5), 1311–1327.

(30) Pickett, H. M.; Strauss, H. L. *J. Am. Chem. Soc.* **1970**, *92* (25), 7281.

(31) Feig, M. *J. Chem. Theory Comput.* **2008**, *4* (9), 1555−1564.

(32) Smith, P. E. *J. Chem. Phys.* **1999**, *111* (12), 5568–5579.

(33) Kwac, K.; Lee, K. K.; Han, J. B.; Oh, K. I.; Cho, M. *J. Chem. Phys.* **2008**, *128* (10), 105106.

(34) Feig, M. *J. Chem. Theory Comput.* **2007**, *3* (5), 1734–1748.

(35) Chekmarev, D. S.; Ishida, T.; Levy, R. M. *J. Phys. Chem. B* **2004**, *108* (50), 19487–19495.

(36) Swope, W. C.; Pitera, J. W.; Suits, F.; Pitman, M.; Eleftheriou, M.; Fitch, B. G.; Germain, R. S.; Rayshubski, A.; Ward,

T. J. C.; Zhestkov, Y.; Zhou, R. *J. Phys. Chem. B* **2004**, *108* (21), 6582–6594.

(37) Kim, Y. S.; Wang, J. P.; Hochstrasser, R. M. *J. Phys. Chem. B* **2005**, *109* (15), 7511–7521.

(38) Grdadolnik, J.; Grdadolnik, S. G.; Avbelj, F. *J. Phys. Chem. B* **2008**, *112* (9), 2712–2718.

(39) Dadarlat, V. M. *Biophys. J.* **2005**, *89* (3), 1433–1445.

(40) Solov'yov, I. A.; Yakubovich, A. V.; Solov'yov, A. V.; Greiner, W. *Phys. Rev. E* **2006**, *73* (2), 021916.

(41) Bonvin, A.; Boelens, R.; Kaptein, R. *Biopolymers* **1994**, *34* (1), 39–50.

(42) Wilson, K. P.; Black, J. A. F.; Thomson, J. A.; Kim, E. E.; Griffith, J. P.; Navia, M. A.; Murcko, M. A.; Chambers, S. P.; Aldape, R. A.; Raybuck, S. A.; Livingston, D. J. *Nature* **1994**, *370* (6487), 270–275.

(43) Chowdhury, I.; Tharakan, B.; Bhat, G. K. *Comp. Biochem. Physiol. B: Biochem. Mol. Biol.* **2008**, *151* (1), 10–27.

(44) Ghysels, A.; Van Neck, D.; Van Speybroeck, V.; Brooks, B. R.; Waroquier, M. *J. Chem. Phys.* **2009**, *130*, 084107.

CT800489R